3D electrical resistivity tomography of karstified formations using cross-line measurements

Van Hoorde Maurits, Dredging International NV, member of the DEME-group

Hermans Thomas, Stanford University, Geological Sciences, now at University of Liege, Urban and Environmental Engineering, Belgium.

Dumont Gaël, University of Liege, Urban and Environmental Engineering, Belgium.

Nguyen Frédéric, Department of Civil Engineering, KU Leuven, Belgium

Corresponding author:

Hermans Thomas, thomas.hermans@ulg.ac.be

The final version of this article is published in *Engineering Geology*, please cite as

Van Hoorde M., Hermans T., Dumont G., and Nguyen F. 2017. 3D Electrical resistivity tomography of karstified limestone using cross-line measurements. *Engineering Geology*, 220, 123-132. http://dx.doi.org/10.1016/j.enggeo.2017.01.028

Highlights

1) We develop an innovative 3D ERT measurement procedure to image complex 3D resistivity structure
2) The measurements procedure is based on the roll-along technique combined with cross-line measurements in several directions and distances
3) The procedure is optimized to minimize the required equipment and acquisition time on the field
4) We show with synthetic and field measurements the increased imaging capacity of our acquisition procedure compared to 2D parallel lines

Abstract

The acquisition of a full 3D survey on a large area of investigation is difficult, and from a practitioner's point of view, very costly. In high-resolution 3D surveys, the number of electrodes increases rapidly and the total number of electrode combinations becomes very large. In this paper, we propose an innovative 3D acquisition procedure based on the roll-along technique. It makes use of 2D parallel lines with additional cross-line measurements. However, in order to increase the number of directions represented in the data, we propose to use cross-line measurements in several directions. Those cross-line measurements are based on dipole-dipole configurations as commonly used in cross-borehole surveys. We illustrate the method by investigating the subsurface geometry in a karstic environment for a future wind turbine project. We first test our methodology with a numerical benchmark using a synthetic model. Then, we validate it through a field case application to image the 3D geometry of karst features and the top of unaltered bedrock in limestone formations. We analyze the importance of cross-line measuring and analyze their capability for accurate subsurface imaging. The comparison with standard parallel 2D surveys clearly highlighted the added value of the cross-lines measurements to detect those structures. It provides crucial insight in subsurface geometry for the positioning of the future wind turbine foundation. The developed method can provide a useful tool in the design of 3D ERT survey to optimize the amount of information collected within a limited time frame.

Keywords: 3D electrical resistivity tomography, karstic environments, cross-line measurements, electrode configuration

1. Introduction

In the last two decades, electrical resistivity tomography (ERT) has been widely applied in many different contexts such as groundwater resources (e.g., Hermans et al., 2015; Yeh et al., 2015), fault imaging (e.g., Nguyen et al., 2005; Suski et al., 2010) and geotechnical applications (e.g., Chambers et al., 2013; Sauret et al., 2015). The wide range of applications of ERT is a result of the large number of parameters influencing the electrical resistivity of the subsurface (porosity, fractures, rock/soil type, saturation, temperature, fluid electrical conductivity, etc.) and the robustness of the method. Because of the simplicity of field implementation, requiring only one to two people for a couple of hours, 2D surveys are not time-consuming and relatively cost-effective. In addition, acquisition times have drastically decreased with the advent of multi-channel systems and automated switching systems (LaBrecque et al., 1996). Nevertheless, one of the major drawbacks of 2D surveys is the underlying assumption that the subsurface is actually 2.5D, i.e. that electrical resistivity is constant in the direction perpendicular to the profile. This assumption allows to successfully reduce the complexity of forward modeling from 3D to 2D using a Fourier-cosine transformation (Dey and Morrison, 1979). Most interpretation software, commercial or academic, uses this assumption in the inversion of 2D data sets.

The 2.5D assumption can be valid for certain conditions (profile perpendicular to main geological structures, relatively homogeneous subsurface), but it can also lead to distorted and misleading results in strongly variable and heterogeneous environments (e.g. Bentley and Gharibi, 2004; Nimmer et al., 2008), such as encountered in karstic settings. In such cases or when a detailed mapping of the subsurface is required, 3D acquisition and inversion techniques must be considered. This remark is particularly true for karstic hazard where the 3D nature of the dissolution processes makes the 2.5D hypothesis of the subsurface much weaker than for fault imaging for example.

In most cases, the acquisition of a full 3D survey on a large area of investigation is difficult and, from a practitioner's point of view, very costly. The number of electrodes increases rapidly, the time to acquire a complete data set and the required equipment are prohibitive. In most applications, 3D surveys with a substantial number of electrodes (more than 100) are not full 3D surveys but limited to the two main directions and the cross-diagonal (e.g., Li and Oldenburg, 1994; Kaufmann and Deceuster; 2007). Fiandaca et al. (2010) developed a 3D acquisition procedure called maximum yield grid which limits the number of pairs of electrode used for current injection and therefore reduce the impact on vulnerable surfaces such as archeological sites (Capizzi et al., 2012).

However, to limit logistic constraints and optimize the acquisition time, 3D surveys are generally designed as extensions of 2D surveys and can be performed with a limited amount of electrodes connected to the resistivity meter at a certain moment in time. The most common solution is then to deploy 2D parallel lines. The acquisition is 2D but the data are processed using a 3D inversion code which accounts for heterogeneity in the direction perpendicular to the 2D lines (e.g., Chambers et al., 2011; Orfanos and Apostolopoulos, 2011; Ustra et al., 2012). The extension in both directions depends on the objectives of the investigation. Rücker et al. (2009b) used 12 long lines of 140 electrodes with 3 m electrode spacing and 15 m line spacing, covering an area of about 70 000 m^2 to investigate a gold heap. In contrast, Papadopoulos (2010) carried out a square survey of 26 lines of 26 electrodes with 1 m electrode- and line-spacing in tumuli investigations.

2D parallel surveys are relatively fast given the high number of electrodes generally used, but they suffer from the limited 2D acquisition. Indeed the sensitivity to resistivity changes in the perpendicular direction rapidly decreases for 2D surveys and most perpendicular structures might be poorly imaged. To overcome this limitation, many authors have proposed to use 2D lines in two orthogonal directions in order to acquire data in more than one direction (e.g., Bentley and Gharibi, 2004; Berge and Drahor, 2011; Negri et al. 2008) Those studies have shown that the inversion results of 2D orthogonal setups were more satisfactory, except if the direction of the anomaly was already known or the electrode interspacing was sufficiently small. For large domains, Rucker et al. (2009a) have shown that inverting the whole data set at once yielded better results than inversions on sub-domains.

To consider data collection in more than two directions, some authors have also proposed radial or star shaped surveys (e.g., Tsourlos et al., 2014; Nyquist and Roth, 2005), providing more information on the heterogeneity of the subsurface in the central part of the investigated zone Non-standard 3D surveys, such has C-shape or L-shape (e.g., Chavez et al., 2014), square-shape (Argote-Espino et al., 2013) or ring-shape (Brunner et al., 1999) have also been tested in complex environments where it is not possible to use electrodes on a large area.

However, both orthogonal and radial surveys ask for additional field work by increasing the number of lines to acquire. Dahlin et al. (2002), in contrast, proposed a roll-along methodology in the orthogonal directions to acquire simultaneously 2D parallel lines and orthogonal measurements. It proposes to set-up several parallel lines at the same time and to acquire cross-line measurements in the orthogonal direction using electrodes already connected on the parallel lines. When the first line has been acquired, it is removed and placed next to the last line as in classical roll-along. Dahlin et al. (2002) tested the procedure with a pole-pole survey on a 17 lines survey with 21 electrodes, using 6 cross-line measurements (7 cables) in the orthogonal direction only. This procedure reduces significantly the time spent on the field but provides a data set less complete than a full orthogonal survey and still limits the number of measurement directions during data acquisition.

In this paper, we propose an innovative 3D acquisition procedure based on the roll-along technique of Dahlin et al. (2002). It makes use of 2D parallel lines with additional cross-line measurements. However, in order to increase the number of directions represented in the data, we propose to use cross-line measurements in several directions as proposed in Cho and Yeom (2007) for imaging seepage in an embankment. Those cross-line measurements are based on dipole-dipole configurations as commonly used in cross-borehole surveys. We illustrate the method by investigating the subsurface geometry in a karstic environment for a future wind turbine project. We first describe the field site and the geological context. Then, the designed acquisition and processing procedure is described and assessed by numerical benchmark modeling, using a synthetic model. We applied our validated methodology to the field case to image the top of the unaltered limestone formation and to characterize the 3D geometry of karst features. We then discuss the importance of cross-line measuring and analyze its capability and optimal setup for correct subsurface geometry imaging.

2. Field site

The test site is located in the Couvin region, Belgium (Figure 1). It is a large area where a wind turbine construction project is ongoing. As a preliminary study, a 2D electrical resistivity tomography profile was performed by a private company (64 electrodes, 5 m spacing, NW-SE direction) at the assumed location of each future wind turbine location. A large, medium resistivity value anomaly (150-200 Ω.m) was detected beneath the location of one of the future wind turbines. This anomaly was interpreted as an entity where limestone is heavily altered and is supposedly linked to karstic phenomena present in the subsurface (see section 2.2).

Standard geotechnical investigations (such as cone penetration tests) would provide only punctual information. Ideally, in such complex geo-hazardous environments, a 3D integrated site investigation should be executed to construct a 3D subsurface geological model which can support civil engineering and strategic design (e.g., Song et al., 2012; Ismail and Anderson, 2012). This concept was the motivation to conduct a 3D ERT survey at the location of the future wind turbine.

2.1.Geology

The survey site region is located at the southwestern edge of the synclinorium of Dinant, a geological structure composed of a succession of folded carbonate and terrigenous rocks (Marion and Barchy, 1999b). The oldest lithostratigraphic unit in the study area is composed of the formations of Saint-Joseph and of Eau Noire, consisting of layers of shale and thin limestone. The second oldest formation is the formation of Couvin. It consists of very thick and compact succession of limestone layers.. The youngest formation is the formation of Jemelle, mostly consisting of shale layers (Marion and Barchy, 1999b).

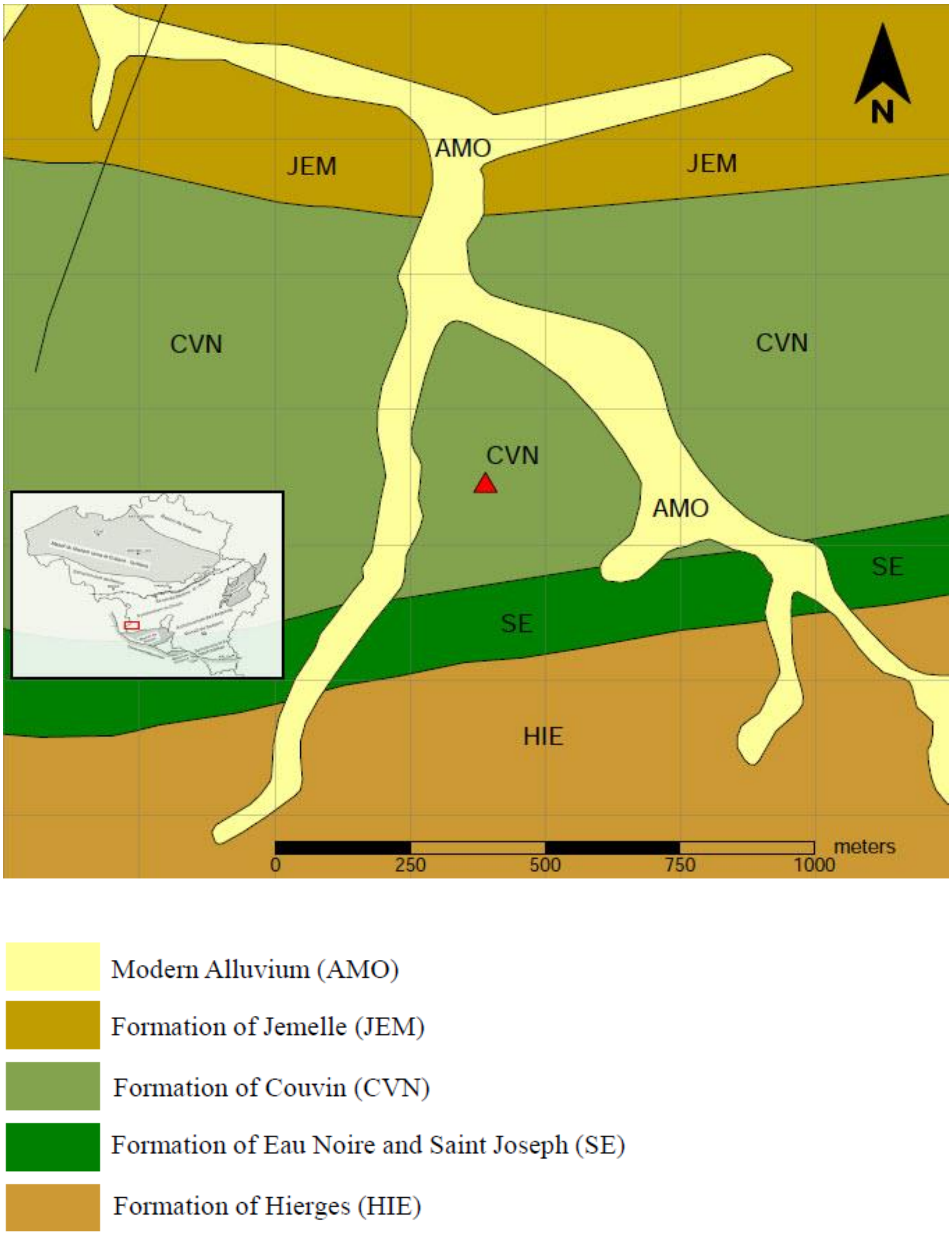

<u>Figure 1:</u> Geological map of the site location. Red triangle represents the study area (modified after Marion and Barchy, 1999a).

2.2. Karst characterization

Shallow karsts constitute a serious hazard to existing constructions and for civil engineering projects due to the risk of resurgence, subsurface sinkhole development and subsidence (Sabbe, 2005; Samyn et al., 2014). The subsurface geometry thus needs to be very well characterized in a systematic way when constructing in limestone settings (Alija et al., 2013). In the region of the survey site, limestone can be locally highly fractured and karstified. Karst features are generally filled with younger clayey sandstones and sediments (Marion and Barchy, 1999b) and can be reactivated due to the present hydrogeological setting.

Karst features mostly develop in association with discontinuity planes (joints) by progressive dissolution processes occurring under low hydraulic gradient. A soft weathering residue with very high porosity (up to 50% or more), called ghost-rock or isalterite, may remain in place. In areas of intense weathering, paleokarst features may interconnect leading to complex geometries of weathered zones (Mihevc and Stepisnik, 2012). Through isalterite compaction, collapse and transport, underground voids can open and migrate upward, forming sinkholes and typical karstic topography (Kaufmann and Deceuster, 2014).

Ghost rock petrophysical properties show strong variations over short distances (Dubois et al., 2014). Kaufmann and Deceuster (2014) came to the conclusion that ghost-rock materials present a lower density (down to 4 times less), higher porosity (up to 50 times more) and higher permeability (up to 5 times more) than the surrounding limestone bedrock.

Due to the development of microporosity and suction phenomena, the weathering process in isalterite results in a high saturation ratio, leading to a significant decrease in bulk electrical resistivity. Geoelectrical methods are therefore among the most effective to detect and map karstic structures (Dubois et al., 2015). Resistivity values lower than 50 Ω.m generally correspond to silts and clayey sands at the surface and to highly weathered limestone at depth. Resistivity values between 50 and 250 Ω.m correspond to dryer residual sediments/sandstones or less weathered limestone at depth. Resistivity values larger than 250 Ω.m correspond to competent bedrock. This rather low resistivity value is common for argillaceous limestones and limestones with shale intercalation such those encountered in the study area (Ismail and Anderson, 2012; Kaufmann and Deceuster, 2014).

Although no clear guidelines are prescribed for site investigations on karst landscapes, a systematic approach should be developed to analyze karst environments to assess the risks, establish guidelines for foundation design and avoid urban development in hazardous areas (Pueyo Anchuela et al., 2015, Alija et al., 2013, Perrin et al., 2015). As suggested by Song et al. (2012), ERT can be a valuable method to integrate in risk analysis for geo-hazards occurring in karst regions. It can also serve as a tool for time lapse monitoring and continuous characterization of karst features (Epting et al., 2009).

3. Methods

3.1. ERT survey design and protocol

The main objective of our survey design was to use the ABEM Terrameter LS (4 cables of 16 electrodes) equipment which is routinely used to execute 2D–ERT surveys. It was decided to use a set of 18 parallel lines of 32 electrodes in combination with cross-line electrical resistivity measuring, applying the 3D roll along technique to progress laterally through the designed survey grid, connecting only 64 electrodes at a time. In-line measurements were performed along each line, and cross-line measurements were performed in between parallel lines with a certain offset with respect to a fixed chosen profile. The latter contain 3D resistivity information on the subsoil in between parallel lines. The in-line electrode spacing is 5 m whereas the cross-line electrode spacing is 10 m.

In-line measurements were acquired using a standard dipole-dipole configuration with a dipole spacing $a \leq 20\ m$ and a dipole separation $n \leq 6$ times the dipole spacing, leading to a total number of 436 measurements. The cross-line measuring concept is also based on a dipole-dipole configuration (Figure 2). A dipole-dipole configuration has proven to be the most effective electrode array in mapping complex subsurface geometry such as karst features (Zhou et al., 2000, 2002). The current and potential electrodes are located on two different lines. For all current pairs, a maximum of 8 potential dipoles are considered, ensuring, cross-line measurements at different angles to gather as much 3D information as possible within the setup limits. The process is repeated for dipole spacing equal to 5, 10, 15 and 20 m, leading to a number of measurements equal to 638 for each cross-line pair.

The inter-line spacing is increased and the process is repeated with the next line. In our survey, cross-line measurements were taken at an offset of 20, 40 and 60 m. For large inter-line spacing (40 and 60 m), a long interconnection cable was used to connect the cable to the terrameter unit.

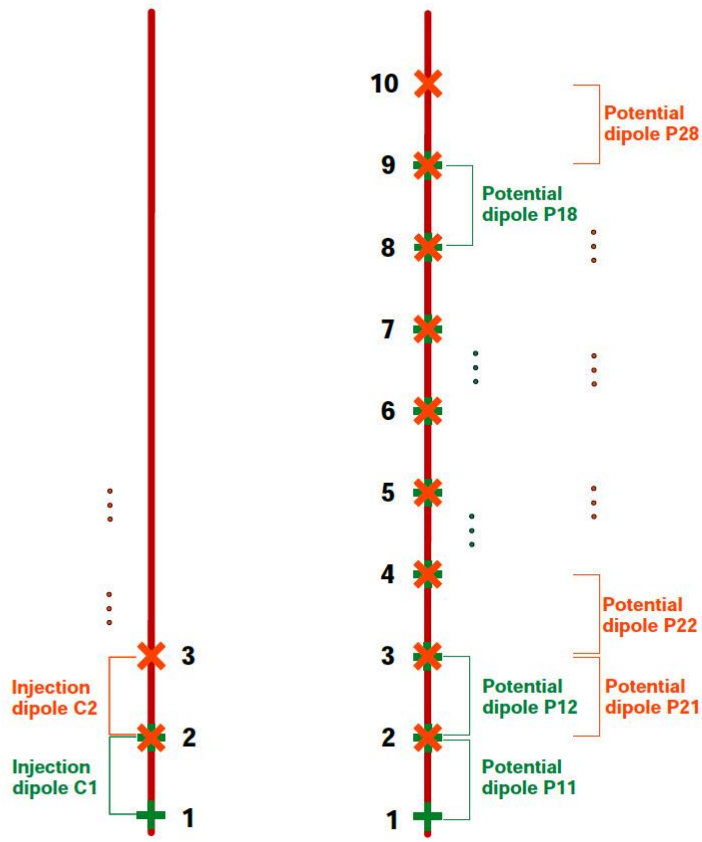

<u>Figure 2:</u> Cross-line measurement concept. Red lines indicate the cables. Current and potential electrode locations for two different injection dipoles are indicated with green and orange crosses respectively.

The overall survey design can be reduced to a set of four unique profiles physically put in place on the survey site (Figure 3). The survey as described here can be performed using 4 electrode cables and a long interconnection cable. However, the use of 8 electrode cables reduces significantly the amount of physical labor during field work. Note that it requires changing the position of the Terrameter LS only 3 times. After data acquisition as depicted in Figure 3E, line 1 can be removed and installed as the next line of the grid (roll-along), while data are being acquired as depicted by F, minimizing acquisition time on the field. Roll-along is routinely applied until the final line is reached. Two different dipole-dipole protocols are used: one in-line (applied to line L1 or line L2) and one cross-line between line 1 and 2 (C12). Figure 4 and Table 1 give a schematic overview of the survey plan. Table 1 also indicates which lines are active (C1, C2, C3, etc.), where the ABEM Terrameter LS is positioned (A12, A45, A6, A7, etc.) and how large the y-spacing is between the active lines (20, 40 or 60 m). The survey design is target and location dependent, it can be altered to any alternative survey design based on different target size, survey site requirements and constraints such as profile length and electrode spacing.

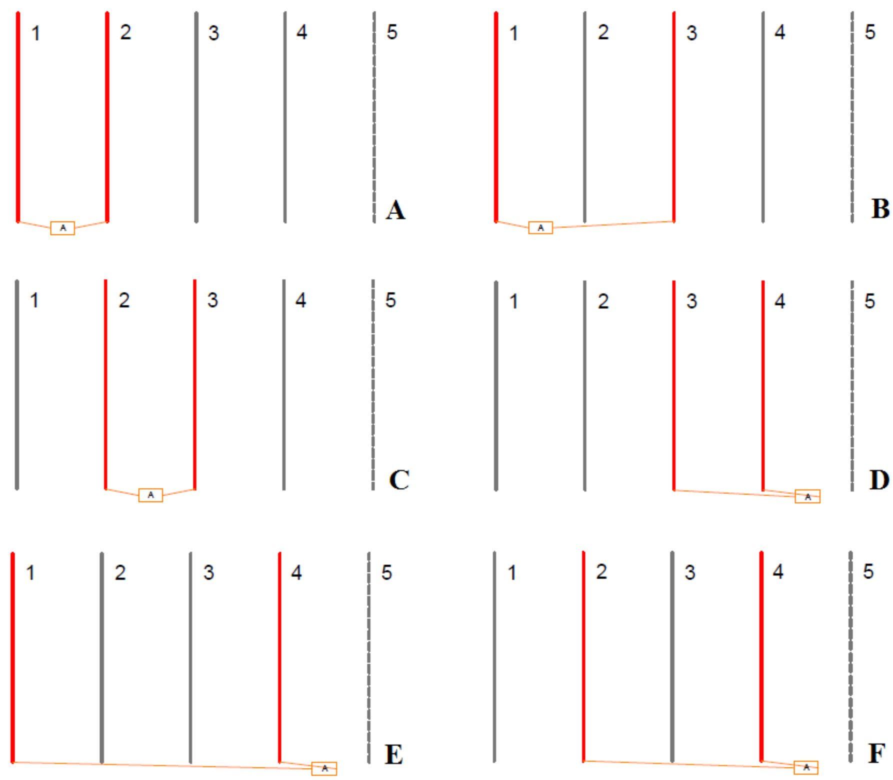

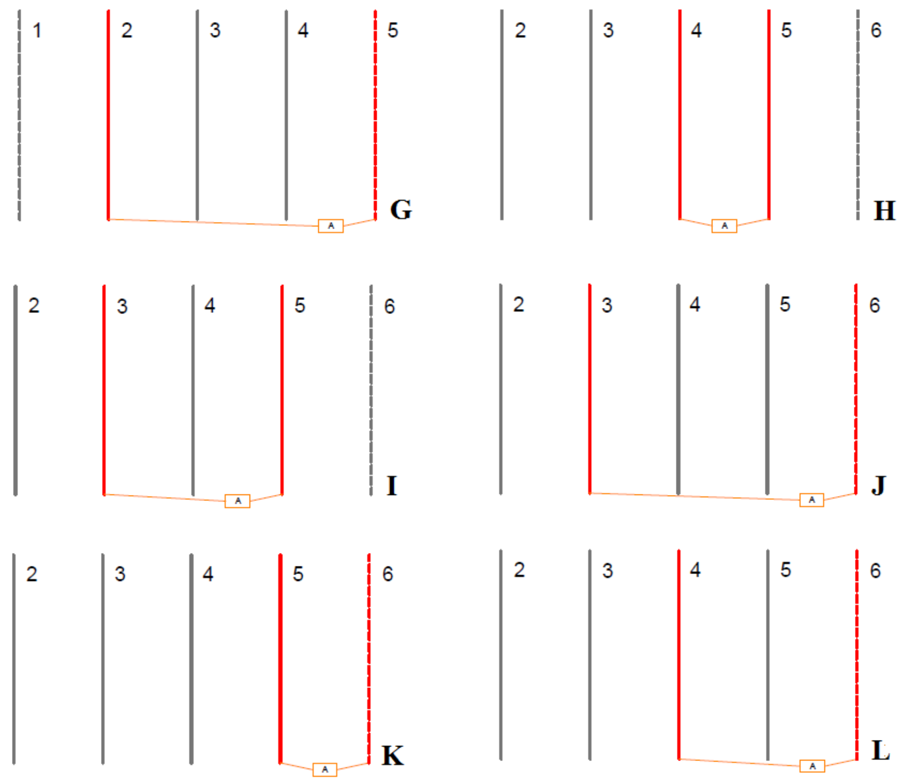

<u>Figure 3:</u> The developed survey design and plan of execution translated in profile line setup.

Position of ABEM + active cables	Y-spacing (m)	Used protocol	Situation in figure 2
A12_C1-C2	20	L1L2C12	A
A12-C1-C3	40	C12	B
A12-C2-C3	20	C12	C
A45-C3-C4	20	L1L2C12	D
A45-C1-C4	60	C12	E
A45-C2-C4	40	C12	F
A45-C2-C5	60	L2C12	G
A45-C4-C5	20	C12	H
A45-C3-C5	40	C12	I
A6-C3-C6	60	L2C12	J
A6-C5-C6	20	C12	K
A6-C4-C6	40	C12	L
A7-C4-C7	60	L2C12	

A7-C6-C7	20	C12	From this point onwards situation J, K and L are routinely performed until the end of the survey grid is reached.
A7-C5-C7	40	C12	
A8-C5-C8	60	L2C12	
A8-C7-C8	20	C12	
A8-C6-C8	40	C12	
A9-C6-C9	60	L2C12	
A9-C8-C9	20	C12	
A9-C7-C9	40	C12	

Table 1: Schematic overview of the survey script. In the left column the position of the ABEM Terrameter LS is indicated by A followed by the line numbers in between which it is positioned. The active cables are indicated by C followed by the line number.

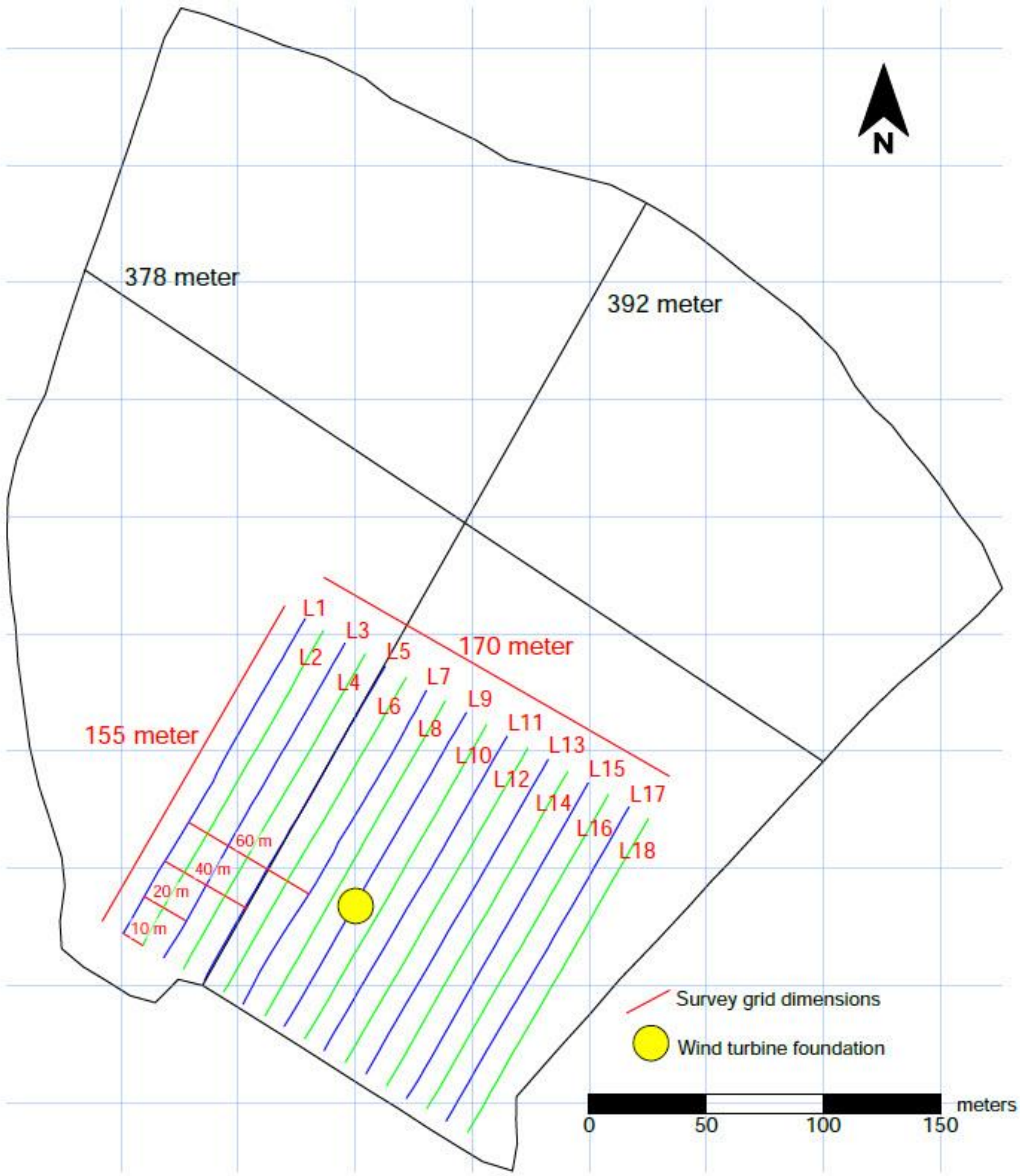

<u>Figure 4:</u> Survey site geometry is depicted by a dark grey line. Blue lines indicate lines of survey 1, green lines indicate lines of survey 2. Together they form the combined survey lay-out. The profile line ID number is indicated in red. The yellow dot is the location of the future wind turbine.

The profile lines were oriented in a north-northeastern direction as perpendicularly to geological structures as possible (Figure 4). Given that the minimum cross-line spacing is 10 m but the minimum offset for crossline measurements is 20 m, it was chosen to split the total survey setup in two surveys of nine profiles 155 m long (5 m electrode spacing).. The second survey line setup has an offset of 10 meter with respect to the first survey setup (Figure 4), i.e. 'in between' the profile lines of survey setup 1Survey 1 and 2 are depicted in Figure 4 by blue and green profile lines respectively. The total grid length in the y-direction is 170 meter. The combined survey grid consists of 576 electrodes, corresponding to a total number of 34644 measurements. All electrodes were precisely positioned using a Trimble G8 GPS system. Note that due to survey site geometry, the wind turbine's location is not perfectly centered.

For acquisition, the delay time was set to 0.2 seconds and the acquisition time to 0.3 seconds. For the same reason, we repeated the measurements maximum 3 times (2 if the error was below 1%). We then used a limit of repeatability error of 1% to accept or reject a given measurement. Injected current was fixed to 200 mA.

We deployed a team of 3 to 4 people on the field. Overall, it took 30-35 minutes to perform a L1L2C12 measurement with the multi-channel ABEM Terrameter LS. For a C12 measurement which measures only 1 crossline setup it took 12-15 minutes. Repositioning the resistivity meter took 5 minutes. Moving a line in the y-direction took 10 minutes, but it can be performed while measurements are running. Mobilizing and de-mobilizing the entire survey equipment spread took 2 hours/day.

3.2. Data processing and inversion

Even though the use of dipole-dipole measurements with relatively large cross-line spacings induced high geometrical factors, the average repeatability error on the apparent resistivity is lower than 0.1%. However, to avoid our inversion to be affected by artifacts, the overall data set (34644 points) was sorted to remove noisy data:

1) Measurements with low or zero current (bad electrode contact) are disregarded as they correspond to injection failures (232 points)
2) Measurements with negative apparent resistivity are removed (2105 points)
3) To ensure sufficient signal to noise ratio, potentials below 0.1 mV were not considered (149 points)
4) Points for which the repeatability error is above 1% are excluded (819 points)

The final data set considered for inversion thus contains 31339 measurements (90% of the full dataset).

To assess the efficiency of cross-line measurements, different combinations of datasets were created (Table 2). One of the data set corresponds to the individual in-line profiles. The other are combinations of in-line and cross-line measurements from survey 1 or survey 1 and 2. The aim of those subsets is to analyze which cross-line measurements are the most informative, in order to reduce acquisition time in future 3D surveys. These 3D informative datasets were inverted using RES3Dinv®. For all considered combinations, topography was included in the inversion process.

All the inversions were carried out with the same inversion parameters. We use a L1 norm on the data to reduce the effect of possible outliers and a L1 norm on the model (Loke et al., 2003) to favor sharp contrasts of resistivity.

Despite, the low variance of the measured apparent resistivity, the final error of the inversion of the full data set is still relatively high (more than 13%). In consequence, the data set was further trimmed post-inversion based on the individual misfit of each simulated measurement versus the observed one. We removed data points with a misfit greater than 20% (5300 data), allowing a decrease of the RMS error to about 6% for the full data sets. For a fair comparison, other subsets were built based on the sorted/trimmed full data set (Table 2). We stopped the inversions when the RMS data misfit reached a value between 5 and 6%.

Survey 1	Combination of datasets	Number of data points in protocol	number of data points after processing
All IL + All CL	9 in-lines + 21 cross-lines	17322	12239
Survey 1+Survey 2			
All IL	18 in-lines	7848	6721
All IL + CL 40	18 in-lines + 14 cross-lines	16780	12925
All IL + CL 60	18 in-lines + 12 cross-lines	15504	12264
All IL + All CL	18 in-lines + 42 cross-lines	34644	25469

Table 2: Different dataset combinations made for three dimensional inversion with RES3Dinv®. ALL IL means all in line, ALL CL all cross-lines, CL # means that only the cross-line with # spacing has been used.

3.3. DOI

We use the depth of investigation index (DOI) as an indicator of the depth below which the model parameters are not constrained by the surface data anymore (Oldenburg and Li, 1999; Oldenborger et al., 2007; Caterina et al., 2013). The DOI index can be calculated for every cell by:

$$DOI(x,z) = \frac{m_{ref1}(x,y,z) - m_{ref2}(x,y,z)}{m_{ref1} - m_{ref2}}$$

with $m_{ref1}(x,y,z)$ and $m_{ref2}(x,y,z)$**,** the inverted model parameters obtained respectively with m_{ref1} and m_{ref2} as reference models and (*x*,*y*,*z*) the coordinates of the cell. m_{ref1} and m_{ref2} have a resistivity respectively ten times smaller and higher than the average apparent resistivity. The relative weight given to the reference model during inversion is equal to 0.05. The DOI index is generally used in its normalized form (DOI_{norm}) by dividing the index vector by its maximum value (DOI_{max}) (Marescot et al. 2003):

$$\mathrm{DOI_{norm}} = \frac{\mathrm{DOI}}{\mathrm{DOI_{MAX}}}$$

$$DOI(x,z) = \frac{m_{ref1}(x,z) - m_{ref2}(x,z)}{m_{ref1} - m_{ref2}}$$

Indexes approaching zero mean that both inversions produce the same electrical structures and therefore that the inverted model is still constrained by the data. Inversely, a DOI approaching one means the model cells are less constrained by the data. A threshold value between 0.1–0.2 is often chosen based on literature to calculate the depth of investigation (Oldenburg and Li, 1999; Marescot et al., 2003; Miller and Routh, 2007).

4. Synthetic model

A numerical benchmark model is first carried out. the objective is to validate if our designed survey method can image an artificially pre-defined 3D geological structure.

4.1. Description of the model

The synthetic model mimics the karstic environment expected at the study site. The numerical geological structure consists of a central ridge of competent limestone with karstic features on the sides (Figure 5). The different geological units are a sediment cover, 10 m thick (55 Ω.m), weathered limestone with debris (450 Ω.m), ghost rock and tertiary sandstone filling karstic features (250-300 Ω.m) and unaltered limestone bedrock (750 - 2500 Ω.m). RES3DMOD is used to numerically simulate the apparent resistivity data corresponding to a pole-pole survey. Those are subsequently used to build dipole-dipole dataset combinations similar to the one described in section *3.2.* We therefore use the detection of the shape and location of the central limestone ridge as an indicator of the performance of the survey, since it is of uttermost importance for the wind turbine project. This characteristic of the model will be highlighted by the 600 Ω.m iso-surface using the isoline methodology (e.g., Chambers et al., 2014b) and a horizontal slice. To enhance the visualization of the ridge, the structures in the first 15 m below the surface are disregarded.

4.2. Inversion results

The full data set is expected to bring the most valuable information on the 3D structure of the model. As it appears in Figure 5, this data set allows to retrieve relatively accurately the location, depth and shape of the ridge in the middle of the model. This observation confirms the survey (in-line and cross-line spacing, number of parallel lines) was correctly designed.

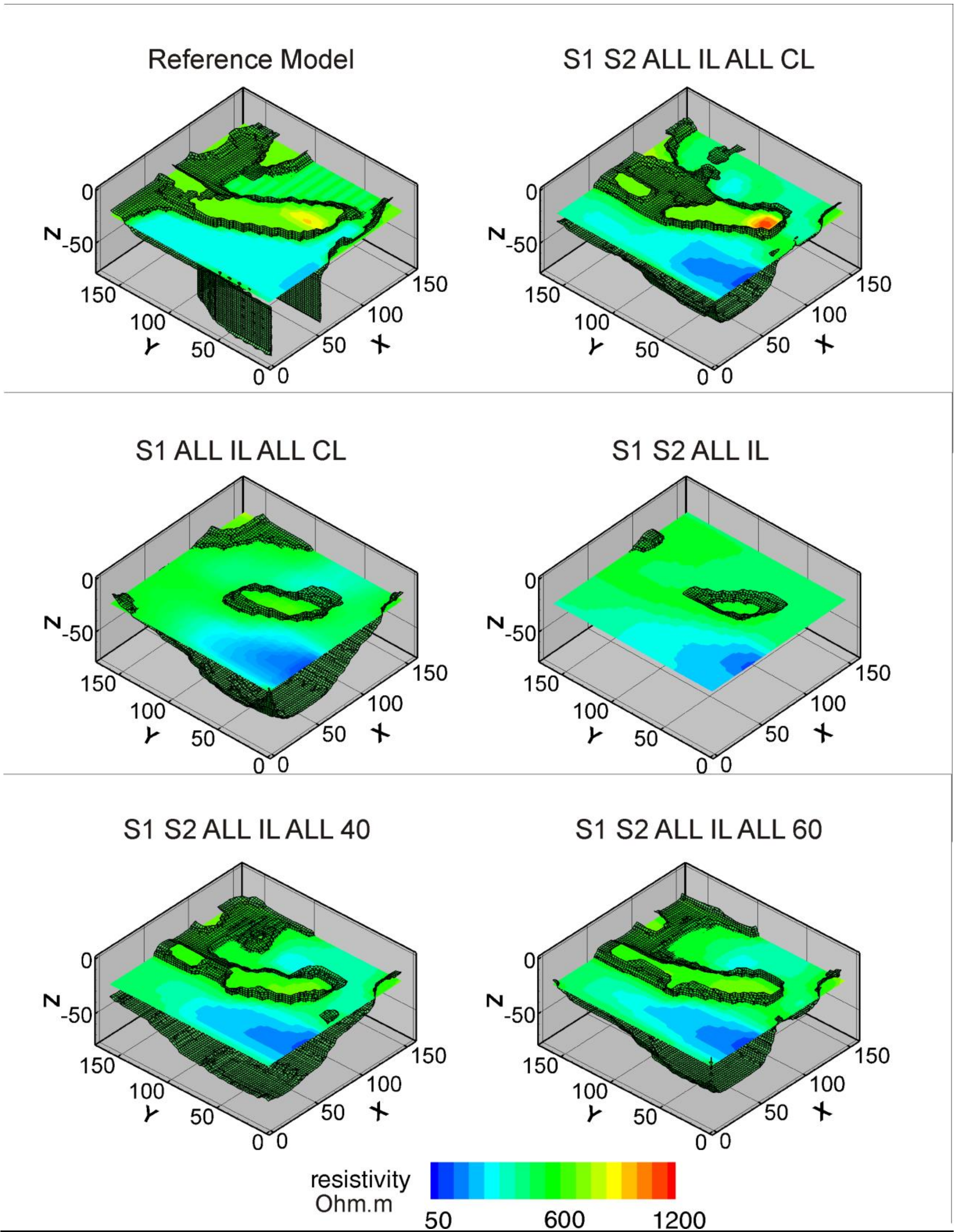

. *The models show a resistivity iso-surface of 600 Ω.m representing the transition to altered limestone* *and a horizontal slice at 23 m depth. The model annotation corresponds to the dataset combination overview provided in table 2.*

All the reduced data sets retrieve less accurately the ridge structure. First, it appears that that the use of a unique survey, i.e. an inter-line spacing of 20 m, is not able to image correctly the subsurface. It detects the low resistive zone located at the origin of the grid and part of the ridge, but not its complex 3D structure. Similarly, the use of the in-line data from both surveys is not able to image correctly the 3D geometry, although general trends are detected. More specifically, the absence of cross-line measurements impedes the detection of the transition to healthy limestone. The good detection of the general trends lies in the orientation of 2D lines perpendicular to the geological structures. Adding cross-line measurements to 2D lines clearly improves the results. In this case, given the depth of the structure, cross-lines 40 m and 60 m are the most informative. They enable us to refine imaging of the 3D structure.

5. Field model

In the inversion of the full data set (Figure 6), a subsurface structure is recognizable with a central ridge of unaltered limestone bedrock at a depth between 225 m TAW and 195 m TAW. On its sides, two karstic features are clearly visible. The first is a large zone of low resistivity value between X = 0 and X = 50 m, the healthy bedrock being detected at a depth of 195 m TAW. The second is a smallest low resistivity zone located between Y = 50 m and Y = 100 m and X = 75 m and X = 150 m.

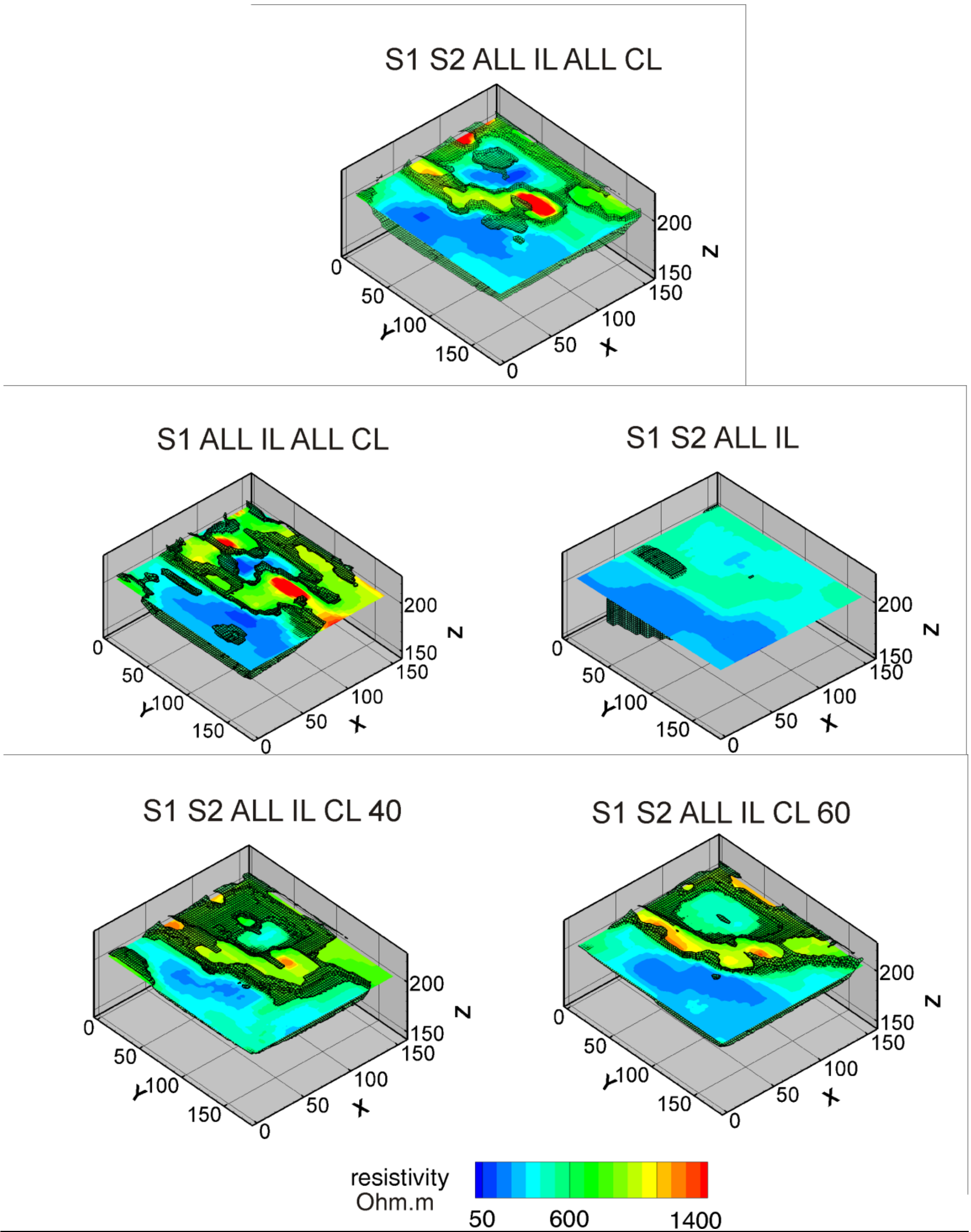

Figure 6: *Field data inversion overview. The models show a resistivity iso-surface of 600 Ω.m representing the transition to altered limestone and a horizontal slice at the elevation of 205 m*

(20 m depth). The model annotation corresponds to the dataset combination overview provided in table 2.

The inversion of reduced data sets confirms the observation made for the synthetic case. Clearly, the use of a spacing of 20 m between parallel lines is not sufficient to resolve the shape and location of the limestone ridge. This subset of data incorrectly locates the ridge and its shape, and adds undesirable high resistivity features in the area. The use of in-line data only qualitatively detects most trends of the subsurface geometry with smaller resistivity contrasts, but the depth of the unaltered bedrock is found deeper down (therefore not visible on the slice in Figure 6)Both inversions with additional cross-line dipoles (40 m and 60 m) manage to image the subsurface geometry as the full data set does. Those data sets image the second low resistivity anomaly with a shape relatively similar to the reference. This observation is probably linked to the depth of the targeted structures. Indeed, the cross-lines 20 m (not shown here), proved to be mainly helpful to image 3D structure in the first meters below the surface (surface deposits).

As expected by the smaller data density at the beginning and ending of each survey line, the DOI index remains small in the central part of the survey grid and increases towards the outer borders (Figure 7). Using the dataset with a larger y-spacing (SI ALL IL ALL CL) induces high DOI index values in the area where 3D geometry is most pronounced, reducing our confidence in the detection of the ridge. The absence of cross-line data (SI S2 ALL IL) also induces a global increase in the DOI index. The use of 40 m cross-line data is in this case the best alternative with respect to the full data set. This dataset is able to capture 3D geometry at the required depth with low DOI index values. Nevertheless, the absence of cross-line data at 20 m separation tends to increase the DOI index at shallow depth. Using only cross-line data with a spacing of 60 m induces a shortage of data in the data-set at shallow and medium depths where 3D structures are present, increasing the DOI index. Those measurements are also characterized by higher geometrical factors and therefore a less favorable signal to noise ratio. This may explain higher DOI indexes observed in the zone corresponding to the first karstic anomaly. However, both inversion clearly identified the contrast between the ridge and the karstic zone. Globally,it can be stated that the central ridge structure observed in the inversions is constrained by the data.

For comparison, the 0.2 DOI limit of individual 2D sections (not shown) has an average depth of 12.5-15 meter in the central part of survey profile lines while it is around 42.5-45 meter for the 3D models. Cross-line data thus have a strong positive effect on the depth of investigation

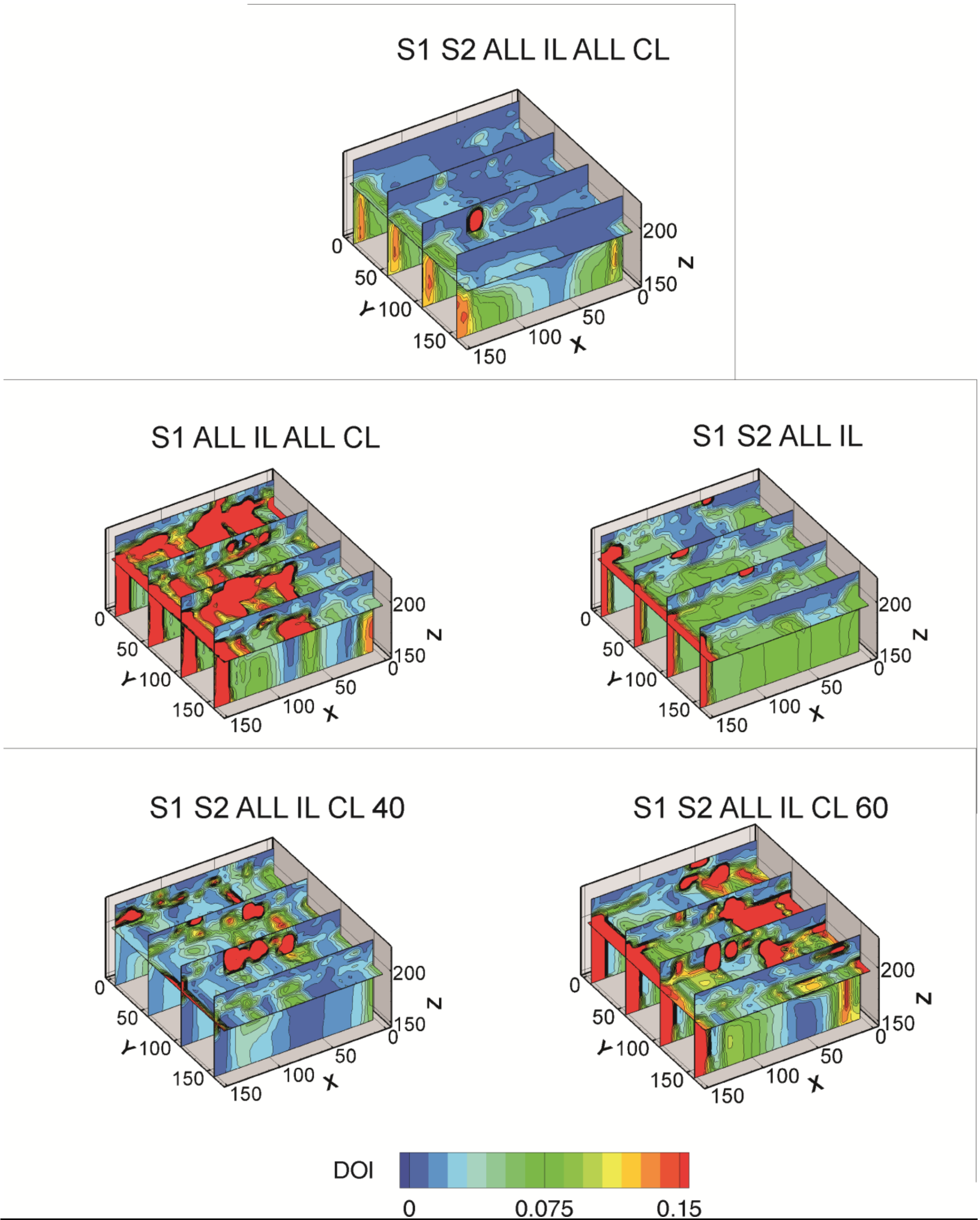

Figure 7: *3D DOI index visualization. The horizontal slice of 200 m TAW is shown. A vertical slice is depicted every 50 m.*

6. Discussion and Conclusion

The most efficient way to conduct a three dimensional resistivity survey is to deploy a set of parallel profile lines. However, the addition of measurements in other direction brings important additional information on the 3D structure of the subsurface. In this paper, we propose an innovative methodology to collect efficiently 3D electrical resistivity surveys. We combined the standard 2D parallel acquisition with cross-line measurements, using the roll-along technique in the perpendicular direction. In contrast to existing procedures, we include more than one direction in cross-line measurements using dipole-dipole configurations similar to what can be done in cross-borehole surveys. This procedure is a convenient and innovative way to execute a 3D informative ERT survey, using the same equipment as for a 2D ERT survey.

We applied this methodology on a synthetic case. It proves that such a data set is informative to image the 3D resistivity structure of the subsurface. Especially, it is important to collect 3D measurements with a depth of investigation coherent with the expected structure of the subsurface. However, the collection of cross-line measurements must not be in detriment of a sufficiently small spacing between parallel lines. The inter-line spacing should not be larger than two times the in-line spacing to avoid unacceptable deterioration to the recovered resistivity model.

The numerical results were validated by a field case study. We acquired on the field the proposed 3D in-line/cross-line surveys to image limestone formations subject to karstic features within the context of a wind turbine project. Our methodology enabled us to successfully image the presence of a central unaltered limestone ridge surrounded by much less competent rock affected by karstic phenomena. The comparison with standard parallel 2D surveys clearly highlighted the added value of the cross-lines measurements to detect those structures. The computation of the depth of investigation index (DOI) has shown that the 3D DOI is 300% larger than the 2D DOI. The cross-line data and 3D inversion have a positive effect on the depth of investigation to constrain the 3D inverted model to greater depths. The produced 3D resistivity models provide a thorough understanding of subsurface geometry, even for non-expert users. In the light of civil engineering purposes, the visual power of these models will greatly help to improve communication between geo-scientists and project engineers.The results provide crucial insight in subsurface geometry for the positioning of a future wind turbine foundation, to the best of our knowledge of the site.

In our case study, a 12-channel ABEM Terrameter LS resistivity meter was used. Time optimized survey parameters greatly decrease survey time without drastically affecting data quality. Indeed, in many cases, adding stacks will slightly decrease the repeatability errors and increase the accuracy, but to a level not sufficient to accept the data for inversion. Using two stacks and a cut-off of 1% in repeatability error appears to be a fast and efficient way to accept/reject data points.

Trying to save survey time, and thereby reduce cost, by decreasing the amount of cross-line measurements should be done only very carefully. The model quality decreases rapidly with decreasing amount of 3D informative data. A survey setup, including in-line measurements and cross-line measurements at 20, 40 and 60 meter should be respected. Using only cross-line data is nevertheless a bad idea. Spatial coverage is not large enough within this survey setup; a basic framework of in-line measurements should therefore always be acquired. If one would like to reduce survey time and costs or if only four cables are available to perform the survey, the best alternative is to use cross-line measurements at 40 m in this specific case. However, this conclusion is likely dependent on the local geology and the targets of the survey. A thorough pre-survey site study should be performed to adjust the survey design to the most suitable setup for site specific conditions.

The mid-scale survey presented in this study took 2 days of survey preparation, 3 days of fieldwork, and an extra week for data processing and reporting. In terms of cost, the 3D survey was about 50% more expensive than a 2D survey of the same dimensions, but it brings more accurate information. Unfortunately, it is difficult to quantify the added value of the information collected.

Future work should concentrate on the optimization of cross-line measurements in order to reduce the acquisition time of such surveys. Efforts should be made to create an integrated site investigation framework for the characterization of geo-hazardous environments affected by karst features in the light of pre-construction risk analysis, combining geotechnical and geophysical survey methods such as cone penetration testing in combination with 3D ERT and seismic surveying.

ACKNOWLEDGEMENT

We would like to thank the geophysical exploration company G-tec S.A. for giving us the opportunity to work on the field site, and for their help on the field for collecting the data. We would like to thank Windvision, for providing us the permission to work on their site and their interest in this work. We thank the Belgian American Educational Foundation and Wallonia-Brussels International for their financial support of T. Hermans. We thank Dale Rucker and the Editor Janusz Wasowski for their helpful comments on the manuscript.

REFERENCES

Alija, S., Torrijo, F.J., Quinta-Ferreira, M., 2013. Geological engineering problems associated with tunnel construction in karst rock masses: The case of Gavarres tunnel (Spain). Engineering Geology 157, 103–111. doi:10.1016/j.enggeo.2013.02.010

Argote-Espino, D., Tejero-Andrade, A., Cifuentes-Nava, G., Iriarte, L., Farías, S., Chávez, R.E., López, F., 2013. 3D electrical prospection in the archaeological site of El Pahñú, Hidalgo State, Central Mexico. Journal of Archaeological Science 40, 1213–1223. doi:10.1016/j.jas.2012.08.034

Bentley, L.R., Gharibi, M., 2004. Two- and three-dimensional electrical resistivity imaging at a heterogeneous remediation site. GEOPHYSICS 69, 674–680. doi:10.1190/1.1759453

Berge, M.A., Drahor, M.G., 2011. Electrical Resistivity Tomography Investigations of MultiLayered Archaeological Settlements: Part I - Modelling: ERT Investigations of Multilayered Settlements: Part I - Modelling. Archaeological Prospection 18, 159–171. doi:10.1002/arp.414

Brunner, I., Friedel, S., Jacobs, F., Danckwardt, E., 1999. Investigation of a Tertiary maar structure using three-dimensional resistivity imaging. Geophysical Journal International 136, 771–780.

Capizzi, R., Martorana, R., Messina, P., Cosentino, P.L., 2012. Geophysical and geotechnical investigations to support the restoration project of the Roman “Villa del Casale”, Piazza Armerina, Sicily, Italy. Near Surface Geophysics 10, 145–160. doi:10.3997/1873-0604.2011038

Caterina, D., Beaujean, J., Robert, T., Nguyen, F., 2013. A comparison study of different image appraisal tools for electrical resistivity tomography. Near Surface Geophysics 11, 639–657. doi:10.3997/1873-0604.2013022

Chambers, J.E., Wilkinson, P.B., Kuras, O., Ford, J.R., Gunn, D.A., Meldrum, P.I., Pennington, C.V.L., Weller, A.L., Hobbs, P.R.N., Ogilvy, R.D., 2011. Three-dimensional geophysical anatomy of an active landslide in Lias Group mudrocks, Cleveland Basin, UK. Geomorphology 125, 472–484. doi:10.1016/j.geomorph.2010.09.017

Chambers, J.E., Wilkinson, P.B., Penn, S., Meldrum, P.I., Kuras, O., Loke, M.H., Gunn, D.A., 2013. River terrace sand and gravel deposit reserve estimation using three-dimensional electrical resistivity tomography for bedrock surface detection. Journal of Applied Geophysics 93, 25–32. doi:10.1016/j.jappgeo.2013.03.002

Chambers, J.E., Wilkinson, P.B., Uhlemann, S., Sorensen, J.P.R., Roberts, C., Newell, A.J., Ward, W.O.C., Binley, A., Williams, P.J., Gooddy, D.C., Old, G., Bai, L., 2014. Derivation of lowland riparian wetland deposit architecture using geophysical image analysis and interface detection. Water Resources Research 50, 5886–5905. doi:10.1002/2014WR015643

Chávez, R.E., Cifuentes-Nava, G., Hernández-Quintero, J.E., Vargas, D., Tejero, A., 2014. Special 3D electric resistivity tomography (ERT) array applied to detect buried fractures on urban areas: San Antonio Tecómitl, Milpa Alta, México. Geofísica internacional 53, 425–434.

Cho, I.-K., Yeom, J.-Y., 2007. Crossline resistivity tomography for the delineation of anomalous seepage pathways in an embankment dam. GEOPHYSICS 72, G31–G38. doi:10.1190/1.2435200

Dahlin, T., Bernstone, C., Loke, M.H., 2002. A 3-D resistivity investigation of a contaminated site at Lernacken, Sweden. GEOPHYSICS 67, 1692–1700. doi:10.1190/1.1527070

Dey, A., Morrison, H.F., 1979. Resistivity modeling for arbitrarily shaped two-dimensional structures. Geophysical Prospecting 27, 106–136.

Dubois, C., Deceuster, J., Kaufmann, O., Rowberry, M.D., 2015. A New Method to Quantify Carbonate Rock Weathering. Mathematical Geosciences 47, 889–935. doi:10.1007/s11004-014-9581-7

Dubois, C., Quinif, Y., Baele, J.-M., Barriquand, L., Bini, A., Bruxelles, L., Dandurand, G., Havron, C., Kaufmann, O., Lans, B., Maire, R., Martin, J., Rodet, J., Rowberry, M.D., Tognini, P., Vergari, A., 2014. The process of ghost-rock karstification and its role in the formation of cave systems. Earth-Science Reviews 131, 116–148. doi:10.1016/j.earscirev.2014.01.006

Epting, J., Huggenberger, P., Glur, L., 2009. Integrated investigations of karst phenomena in urban environments. Engineering Geology 109, 273–289. doi:10.1016/j.enggeo.2009.08.013

Fiandaca, G., Martorana, R., Messina, P., Cosentino, P.L., 2010. The MYG methodology to carry out 3D electrical resistivity tomography on media covered by vulnerable surfaces of artistic value. Il Nuovo Cimento B 125, 711–718.

Hermans, T., Nguyen, F., Caers, J., 2015. Uncertainty in training image-based inversion of hydraulic head data constrained to ERT data: Workflow and case study. Water Resources Research 51, 5332–5352. doi:10.1002/2014WR016460

Ismail, A., Anderson, N., 2012. 2-D and 3-D Resistivity Imaging of Karst Sites in Missouri, USA. Environmental & Engineering Geoscience 18, 281–293.

Kaufmann, O., Deceuster, J., 2014. Detection and mapping of ghost-rock features in the Tournaisis area through geophysical methods—an overview. Geologica Belgica 17, 17–26.

Kaufmann, O., Deceuster, J., 2007. A 3D resistivity tomography study of a LNAPL plume near a gas station at Brugelette (Belgium). Journal of Environmental & Engineering Geophysics 12, 207–219.

LaBrecque, D.J., Ramirez, A., Daily, W., Binley, A., Schima, S.A., 1996. ERT monitoring of environmental remediation processes. Measurement Science and Technology 7, 375–383.

Loke, M.H., Acworth, I., Dahlin, T., 2003. A comparison of smooth and blocky inversion methods in 2D electrical imaging surveys. Exploration Geophysics 34, 182–187. doi:10.1071/EG03182

Marescot, L., Loke, M.H., Chapellier, D., Delaloye, R., Lambiel, C., Reynard, E., 2003. Assessing reliability of 2D resistivity imaging in mountain permafrost studies using the depth of investigation index method. Near Surface Geophysics 1, 57–67.

Marion, J.-M., Barchy, L., 1999a. Carte géologique de Wallonie, Chimay-Couvin 57/7-8. Carte Géologique de Wallonie.

Marion, J.-M., Barchy, L., 1999b. Carte géologique de Wallonie, Chimay-Couvin 57/7-8. Notice Explicative. Carte Géologique de Wallonie.

Mihevc, A., Stepisnik, U., 2012. Electrical resistivity imaging of cave Divaska Jama, Slovenia. Journal of cave and karst studies 74, 235–242.

Miller, C.R., Routh, P.S., 2007. Resolution analysis of geophysical images: Comparison between point spread function and region of data influence measures. Geophysical Prospecting 55, 835–852. doi:10.1111/j.1365-2478.2007.00640.x

Negri, S., Leucci, G., Mazzone, F., 2008. High resolution 3D ERT to help GPR data interpretation for researching archaeological items in a geologically complex subsurface. Journal of Applied Geophysics 65, 111–120. doi:10.1016/j.jappgeo.2008.06.004

Nguyen, F., Garambois, S., Jongmans, D., Pirard, E., Loke, M., 2005. Image processing of 2D resistivity data for imaging faults. Journal of applied geophysics 57, 260–277.

Nimmer, R.E., Osiensky, J.L., Binley, A.M., Williams, B.C., 2008. Three-dimensional effects causing artifacts in two-dimensional, cross-borehole, electrical imaging. Journal of Hydrology 359, 59–70. doi:10.1016/j.jhydrol.2008.06.022

Nyquist, J.E., Roth, M.J.S., 2005. Improved 3D pole-dipole resistivity surveys using radial measurement pairs. Geophysical Research Letters 32, L21416. doi:10.1029/2005GL024153

Oldenborger, G.A., Routh, P.S., Knoll, M.D., 2007. Model reliability for 3D electrical resistivity tomography: application oft he volume of investigation index to a time-lapse monitoring experiment. Geophysics, 72(4), F167-F175.

Oldenburg, D.W., Li, Y., 1999. Estimating depth of investigation in DC resistivity and IP surveys. Geophysics 64, 403–416.

Oldenburg, D.W., Li, Y., 1994. Inversion of 3-D resistivity data using an approximate inverse mapping. Geophysical Journal International 116, 527–537.

Orfanos, C., Apostolopoulos, G., 2011. 2D–3D resistivity and microgravity measurements for the detection of an ancient tunnel in the Lavrion area, Greece. Near Surface Geophysics

9, 449–457. doi:10.3997/1873-0604.2011024

Papadopoulos, N.G., Yi, M.-J., Kim, J.-H., Tsourlos, P., Tsokas, G.N., 2010. Geophysical investigation of tumuli by means of surface 3D Electrical Resistivity Tomography. Journal of Applied Geophysics 70, 192–205. doi:10.1016/j.jappgeo.2009.12.001

Perrin, J., Cartannaz, C., Noury, G., Vanoudheusden, E., 2015. A multicriteria approach to karst subsidence hazard mapping supported by weights-of-evidence analysis. Engineering Geology 197, 296–305. doi:10.1016/j.enggeo.2015.09.001

Pueyo Anchuela, ó., Casas Sainz, A.M., Pocoví Juan, A., Gil Garbí, H., 2015. Assessing karst hazards in urbanized areas. Case study and methodological considerations in the mantle karst from Zaragoza city (NE Spain). Engineering Geology 184, 29–42. doi:10.1016/j.enggeo.2014.10.025

Rucker, D.F., Levitt, M.T., Greenwood, W.J., 2009a. Three-dimensional electrical resistivity model of a nuclear waste disposal site. Journal of Applied Geophysics, 69, 150-164.

Rucker, D.F., Schindler, A., Levitt, M.T., Glaser, D.R., 2009b. Three-dimensional electrical resistivity imaging of a gold heap. Hydrometallurgy 98, 267–275. doi:10.1016/j.hydromet.2009.05.011

Sabbe, A., 2005. Le risque karstique dans les constructions d'habitations - propositions de mitigation, in: Karst et Aménagements Du Territoire. Presented at the Karst et Aménagements du territoire.

Samyn, K., Mathieu, F., Bitri, A., Nachbaur, A., Closset, L., 2014. Integrated geophysical approach in assessing karst presence and sinkhole susceptibility along flood-protection dykes of the Loire River, Orléans, France. Engineering Geology 183, 170–184.

doi:10.1016/j.enggeo.2014.10.013

Sauret, E.S.G., Beaujean, J., Nguyen, F., Wildemeersch, S., Brouyere, S., 2015. Characterization of superficial deposits using electrical resistivity tomography (ERT) and horizontal-to-vertical spectral ratio (HVSR) geophysical methods: A case study. Journal of Applied Geophysics 121, 140–148. doi:10.1016/j.jappgeo.2015.07.012

Song, K.-I., Cho, G.-C., Chang, S.-B., 2012. Identification, remediation, and analysis of karst sinkholes in the longest railroad tunnel in South Korea. Engineering Geology 135-136, 92–105. doi:10.1016/j.enggeo.2012.02.018

Suski, B., Brocard, G., Authemayou, C., Muralles, B.C., Teyssier, C., Holliger, K., 2010. Localization and characterization of an active fault in an urbanized area in central Guatemala by means of geoelectrical imaging. Tectonophysics 480, 88–98. doi:10.1016/j.tecto.2009.09.028

Tsourlos, P., Papadopoulos, N., Yi, M.-J., Kim, J.-H., Tsokas, G., 2014. Comparison of measuring strategies for the 3-D electrical resistivity imaging of tumuli. Journal of Applied Geophysics 101, 77–85. doi:10.1016/j.jappgeo.2013.11.003

Ustra, A.T., Elis, V.R., Mondelli, G., Zuquette, L.V., Giacheti, H.L., 2012. Case study: a 3D resistivity and induced polarization imaging from downstream a waste disposal site in Brazil. Environmental Earth Sciences 66, 763–772. doi:10.1007/s12665-011-1284-5

Yeh, H.-F., Lin, H.-I., Wu, C.-S., Hsu, K.-C., Lee, J.-W., Lee, C.-H., 2015. Electrical resistivity tomography applied to groundwater aquifer at downstream of Chih-Ben Creek basin, Taiwan. Environmental Earth Sciences 73, 4681–4687. doi:10.1007/s12665-014-3752-1

Zhou, W., Beck, B., Adams, A., 2002. Effective electrode array in mapping karst hazards in electrical resistivity tomography. Environmental Geology 42, 922–928. doi:10.1007/s00254-002-0594-z

Zhou, W., Beck, B.F., Stephenson, J.B., 2000. Reliability of dipole-dipole electrical resistivity tomography for defining depth to bedrock in covered karst terranes. Environmental Geology 39, 760–766.